

Electronic and ionic conductivities in superionic Li_4C_{60}

D. Quintavalle,¹ B. G. Márkus,² A. Jánosy,¹ F. Simon,^{2,*} G. Klupp,³
M. A. Györi,³ K. Kamarás,³ G. Magnani,⁴ D. Pontiroli,⁴ and M. Riccò⁴

¹*Budapest University of Technology and Economics,
Institute of Physics and Condensed Matter Physics Research Group of the
Hungarian Academy of Sciences, H-1521, Budapest P.O. Box 91, Hungary[†]*

²*Department of Physics, Budapest University of Technology and Economics and MTA-BME
Lendület Spintronics Research Group (PROSPIN), P.O. Box 91, H-1521 Budapest, Hungary*

³*Institute for Solid State Physics and Optics, Wigner Research Centre for Physics,
Hungarian Academy of Sciences, P.O. Box 49, H-1525 Budapest, Hungary*

⁴*Dipartimento di Fisica e Scienze della Terra, Università degli Studi di Parma, Via G. Usberti 7/a, 43124 Parma, Italy*

The 10 GHz microwave conductivity, $\sigma(T)$ and high field, 222 GHz electron spin resonance (HF-ESR) of Li_4C_{60} fulleride is measured in a wide temperature range. We suggest that the majority of ESR active sites and at least some of the charge carriers for $\sigma(T)$ are electrons bound to a small concentration of surplus or vacancy ions in the polymer phase. Both $\sigma(T)$ and the ESR line shape depend on ionic motion. A change of the activation energy of $\sigma(T)$ at 125 K coincides with the onset of the ionic DC conductivity. The ESR line shape is determined mainly by Li ionic motion within octahedral voids below 150 K. At higher temperatures, fluctuations due to ionic diffusion change the environment of defects from axial to effectively isotropic on the ESR time scale. $\sigma(T)$ data up to 700 K through the depolymerization transition confirm that the monomeric phase of Li_4C_{60} is a metal.

PACS numbers: 61.48.+c, 76.30.Pk, 76.30.-v, 78.30.-j

I. INTRODUCTION

C_{60} fullerene molecules form polymeric structures with unusual phenomena, such as e.g. metallic conductivity and antiferromagnetic order along chains¹. Neutral C_{60} is polymerized by a light² or pressure³ induced [2+2] cycloaddition reaction. In these one- and two-dimensional polymeric structures four-membered carbon rings interconnect the fullerene molecules. The polymerization of C_{60}^{n-} anions is spontaneous in alkali intercalated fulleride salts. The structure of these polymers depends on the fulleride charge, n . [2 + 2] cycloaddition is favored for low values of n , like in AC_{60} ($A = \text{K}, \text{Rb}, \text{Cs}$)⁴, while single interfullerene bonds are more stable⁵ for $n \geq 3$ as in Na_4C_{60} and $\text{Na}_2\text{AC}_{60}$ ($A = \text{K}, \text{Rb}$)⁶. The size of the counter-ion also plays a role; e.g. in $\text{Na}_2\text{CsC}_{60}$ a moderate pressure is needed to stabilize the polymeric structure⁷.

Charge storage applications of Li intercalated carbonaceous compounds were proposed as early as 1976 (Ref. 8). In this respect, the Li_4C_{60} fulleride polymer is of special interest. In the 2D polymeric layers of this compound, fullerenes are connected by single bonds along one direction and by [2 + 2] cycloaddition in the other^{9–11}. Li_4C_{60} is a superionic conductor¹² with a high ionic conductivity (0.01 S/cm at 300 K). The ionic conductivity of Li_4C_{60} is intrinsic and it arises from the special structure; at low temperatures half of the Li ions have an unoccupied neighbor site which is easily occupied at higher temperatures¹².

Recently Mg_2C_{60} , a fulleride electronically and structurally similar to Li_4C_{60} , was also found to be an ionic conductor¹³. In the case of alkali fullerides, ionic conduc-

tivity is limited to fullerenes with small alkali metal ions, as the small trigonal aperture connecting interstitial sites within the polymeric framework hinders ionic diffusion. In fulleride crystals with larger alkali metal ions, diffusion requires a reorganization of the fullerene molecular positions. Larger alkali metal ions rearrange or diffuse only at phase transitions or at high temperatures, e.g. above 400 K in Na_2C_{60} [Ref. 14]. The electronic properties under pressure and calorimetric measurements of Li, Na and K doped fullerenes were carried out in detail by the group of Sundqvist *et al.*^{15–19}. The ionic conductivity depends also on other factors than the barrier between sites; counter-intuitively, the DC conductivity of Li_4C_{60} polymer increases under pressure.

Nuclear magnetic resonance (NMR) and electron spin resonance showed that Li_4C_{60} polymer has a non-magnetic, insulating ground state¹⁰ while the high temperature monomer phase is metallic [Ref. 20]. The frequency and temperature dependence of the electric conductivity provides a direct information on the ionic and electronic conductivities and on structural changes. In the Li_4C_{60} polymer, the low frequency conductivity up to 1 MHz is dominated by the ionic contribution¹⁰, while the microwave conductivity is electronic. Microwave frequencies (typically 10 GHz) are well above the characteristic frequency of Li^+ ion movement and far below the plasma edge in fulleride metals²¹ (typically 0.5 – 1 eV, 50 – 100 THz); thus the microwave conductivity is dominated by electronic contributions. Unpaired electrons at Li vacancy and/or Li surplus sites are ESR active and are affected by Li ion diffusion. A complex behavior above 200 K of the electron spin resonance at 9 GHz was reported in a previous study²². The high spectral resolu-

tion at 222.4 GHz of this study allows to follow the onset of Li^+ ion diffusion at the ESR active defect sites.

Here, we present microwave conductivity and high frequency electron spin resonance (HF-ESR) measurements on Li_4C_{60} in the 40 – 700 K temperature range. We study the electronic properties of the polymeric and the monomeric phases with particular attention to the dynamics of electrons in the superionic phase and to the depolymerization process. We find that diffusion of Li^+ ions above 125 K induces an activated electronic conductivity in polymeric Li_4C_{60} . Ion diffusion also explains changes in the HF-ESR spectrum in the same temperature range. We trace the depolymerization process up to 700 K and confirm that the high temperature monomer phase is a good conductor, in accordance with previously reported results²⁰.

II. EXPERIMENTAL

Li_4C_{60} samples were prepared as described previously⁹. A careful X-ray and NMR characterization confirmed the polymeric structure and the stoichiometry Li_xC_{60} with $x = 4$, similarly to the samples investigated in Refs. 12 and 20. For infrared (IR) measurements, the sample was pressed in an Ar filled glove box into KBr pellets. Li and Na doped species were measured in the glove box with a Bruker Alpha spectrometer, K_4C_{60} was measured in an air tight sample holder in a Bruker IFS 66v spectrometer at room temperature with a resolution of 2 cm^{-1} .

Powder samples of Li_4C_{60} were sealed in quartz tubes under 200 mbar He for the microwave conductivity and ESR measurements. Microwave conductivity was measured using the cavity perturbation technique which is well suited for air sensitive powder samples and thus allows the study of alkali fullerene compounds²³. This method is based on the measurement of changes in the quality factor, Q , of a microwave cavity arising from microwave eddy currents in the sample²⁴. The 10 GHz TE011 copper cavity has an unloaded quality factor of $Q_0 \approx 10,000$. A nitrogen gas flow quartz cryostat allowed to vary the sample temperature between 130 K and 700 K while keeping the cavity temperature at 290 K. Measurements in the 40 – 300 K temperature range were performed in a similar cavity placed in a liquid He cryostat. The powder samples were placed at the center of the cavity where in highly conducting samples the electric field is not excluded by depolarization effects. The grain size of the sample was smaller than the microwave penetration depth and the conductivity is proportional to $1/Q - 1/Q_0$ [Ref. 25] where Q and Q_0 are the quality factors of the cavity with and without the sample, respectively²⁶. Only relative variations of the conductivity are measured as the proportionality factor between microwave losses and conductivity depends on the unknown grain size distribution.

High frequency electron spin resonance spectra were

recorded with a home-built spectrometer²⁷ operating at 222.4 GHz (corresponding to 7.93 T for a g -factor of $g = 2$). The maximum output power of the microwave source is 46 mW. Microwave radiation is transmitted by a quasi-optical bridge and is detected with an InSb detector operating at 4.2 K. The spectrometer has a sensitivity of about 3×10^{10} spins / ($10^{-4}\text{ T}\sqrt{\text{Hz}}$). The resolution of ESR lines determined by the homogeneity of the magnet is 0.05 mT.

III. RESULTS AND DISCUSSION

A. Infrared spectroscopy

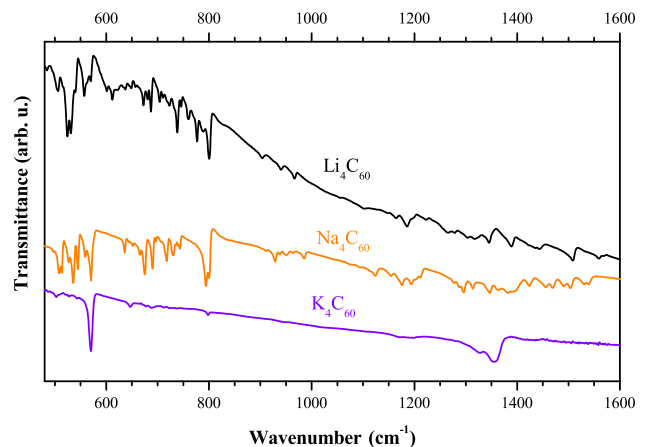


FIG. 1: Room-temperature infrared spectrum of Li_4C_{60} compared to that of Na_4C_{60} and K_4C_{60} , shifted and scaled for clarity. Li_4C_{60} and Na_4C_{60} have similar IR spectra with a mode around 800 cm^{-1} signaling single bonds in the polymer, whereas the IR spectrum of monomeric K_4C_{60} is markedly different.

Fig. 1 shows the infrared (IR) spectrum of Li_4C_{60} and for comparison, the spectra of Na_4C_{60} and K_4C_{60} , where the charge state of the fullerene is also C_{60}^{4-} . The IR spectrum of Li_4C_{60} resembles that of Na_4C_{60} , in agreement with the polymeric nature of both compounds. Na_4C_{60} is a two-dimensional polymer with single bonds²⁸. Polymer formation significantly distorts the C_{60} ball²⁹ and the original icosahedral symmetry of C_{60} is lowered to C_{2h} in Li_4C_{60} [Ref. 9] and C_i in Na_4C_{60} [Ref. 28]. This results in the large number of IR active modes in contrast to the four allowed IR modes of C_{60} . On the other hand, the larger size of the alkali ion hinders the polymer formation in K_4C_{60} . Although there is a Jahn-Teller distortion³⁰ even in this case, the distortion of the C_{60} ball is smaller than in polymers and the IR active modes emerging from the lower symmetry are weak.

The strong band at 800 cm^{-1} in Li_4C_{60} and Na_4C_{60} arises from a single bond between fullerenes³¹ and is not an intramolecular mode. Thus the infrared spectra con-

firm that single bonds are present in the Li_4C_{60} polymer as determined by the structural characterization⁹.

Infrared spectroscopy can in general provide information about the conductivity of materials. In the case of powders in KBr pellets, the effects of light scattering obscure the exact shape of the free-carrier (Drude) absorption, but the signs of metallic character are a strong background absorption and the change of the vibrational bands from Lorentzian to Fano shape^{32,33}. We do not observe any of these effects here, which confirms the absence of such additional spectral weight in the IR spectrum of Li_4C_{60} at room temperature. This invokes that the electronic conductivity is negligible in agreement with Ref. 12. Due to the large mass of the charge carrying ions in fulleride compounds, the Drude peak corresponding to the ionic conductivity is well below the usually accessible frequency of 100 cm^{-1} .

B. Electronic and ionic conductivities in the polymer phase

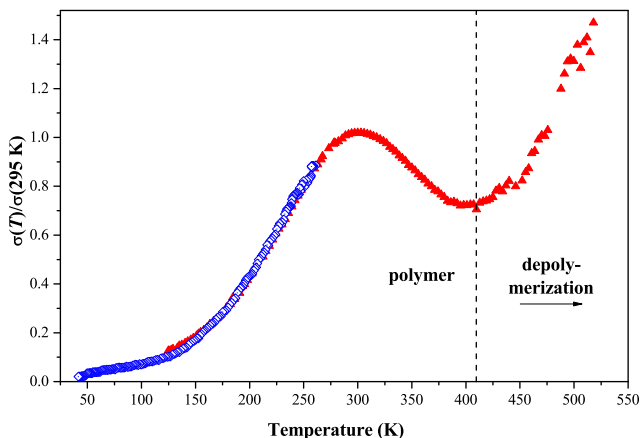


FIG. 2: Temperature dependence of the 10 GHz microwave conductivity of Li_4C_{60} normalized at 295 K. Red triangles: heating (heating rate 0.2 K/s), blue dotted squares: cooling. Unpaired electron concentration increases above 300 K, depolymerization is significant above 400 K.

Fig. 2 shows the temperature dependence of the 10 GHz microwave conductivity, $\sigma(T)$, of Li_4C_{60} normalized to the room temperature value. Data above 260 K are for increasing temperature only. Below 260 K, data taken in heating and cooling are indistinguishable. The conductivity was too small to measure the microwave loss below 40 K. At low temperature, $\sigma(T)$ increases with increasing T ; it has a maximum around 300 K and a minimum at 410 K. Thermal cycles around the polymerization temperature show that the data in Fig. 2 below 400 K corresponds to the polymeric phase. The subsequent rapid increase arises from the onset of depolymerization and is discussed in Sec. III D.

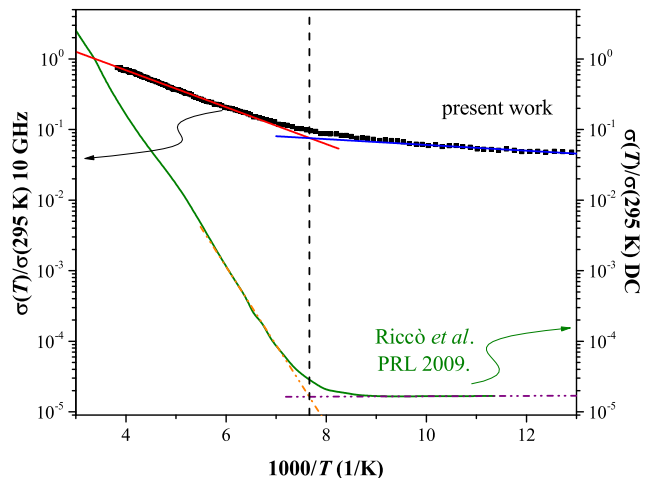


FIG. 3: Arrhenius plot of the 10 GHz (electronic) conductivity in Li_4C_{60} (filled squares, this work) and the DC (ionic) conductivity (solid curve, Ref. 12). The conductivities are normalized to their respective 295 K values. The electronic conductivity is larger than the ionic, however, its absolute value is not known. Straight lines are fits to the data. Note the marked upturn in both electronic and ionic conductivities at about 125 K, which is attributed to the onset of Li^+ diffusion.

TABLE I: The parameters used to fit the activated microwave conductivity of Li_4C_{60} for the $T < 125\text{ K}$ and $T > 125\text{ K}$ regimes.

Regime	σ_0 (arb. u.)	Δ (K)
$T > 125\text{ K}$	$8.7(1) \times 10^{-4}$	603(4)
$T < 125\text{ K}$	$1.7(1) \times 10^{-5}$	90(6)

Fig. 3 compares the low temperature microwave conductivity with the DC conductivity data of Ref. 12 using an Arrhenius presentation. An activated behavior $\sigma(T) = \sigma_0 e^{-\Delta/T}$ with different activation energies, Δ , above and below 125 K fits well the microwave conductivity data. The corresponding parameters are summarized in Table I. The activation energy of the DC ionic conductivity is much larger than for the microwave conductivity. Although the absolute value of the microwave conductivity is not known, it is certainly much larger than the DC conductivity at 125 K, the onset of ionic diffusion and most likely remains larger up to 300 K.

The different temperature dependence of the DC and microwave conductivities suggest these have different origins. In our view¹², above the 125 K onset of Li^+ ionic diffusion to about ambient temperatures the DC conductivity arises mainly from the ionic conductivity, σ_{ion} involving all Li ions. (Sundqvist *et al.*¹⁸ raised, however some doubts about this). On the other hand, we suggest that the microwave conductivity is the electronic conductivity σ_{el} at 10 GHz associated with a small concentration

of charged defects.

There is ample evidence for Li ionic diffusion at ambient temperatures and below^{12,22}. It was observed by the motional narrowing of the ^7Li NMR line and, as explained in Sec. III C, the narrowing of the ESR line above 125 K is also well understood by Li ionic diffusion. The strong temperature and frequency dependence of the DC conductivity supports the dominant role of the ionic contribution³⁴.

The microwave conductivity has an electronic origin; the ionic conduction is negligible at 10 GHz. Except for very low frequencies, the ionic conductivity decreases strongly with frequency. An extrapolation of the low frequency data at 246 K and below shows that σ_{ion} at 10^{10} Hz is well below the sensitivity of the microwave cavity conductivity measurement technique. The total conductivity (i.e. ionic plus electronic) as a function of frequency has a temperature dependent minimum somewhere between 10^6 and 10^9 Hz. From DC to frequencies of the order of 10^6 Hz the conductivity is dominated by the ionic contribution while at higher frequencies the conductivity is due to electrons bound to charged defects.

According to the IR experiment (Sec. III A), the material is essentially an electronic insulator at ambient temperatures; the electronic band gap is large and most electrons do not contribute to the conductivity. We suggest that the electronic conductivity is associated with a small concentration of electrons trapped at defects of the lattice. Li vacancy or Li surplus sites are obvious candidates; for these sites the microwave conductivity and ESR originate from the same electrons. As explained in Sec. III C, the unpaired defect electrons are confined to well defined states at octahedral voids below 125 K. The associated microwave electronic conductivity is due to electron hopping between states in the vicinity of the charged defects. Calorimetric measurements also support this proposal. A contribution to the specific heat was attributed to Li^+ motion within octahedral voids from temperatures as low as 2 K [Ref. 19]. The disorder induced by Li ionic diffusion above 125 K creates new electronic states and allows electronic diffusion of the small concentration of defect electrons to larger distances. This explains the stronger increase of conductivity above the onset of Li ionic diffusion at 125 K.

Finally, we note that one may associate the slowly hopping localized electronic states giving rise to the microwave conductivity of the polymeric phase to small-polarons^{35–38}. Li_4C_{60} is an ionic salt with an insulator ground state. According to HF-ESR results (discussed in Section III C), at low temperatures the excited states are confined to the vicinity of octahedral voids. These localized excitations diffuse slowly as temperature is raised. The small-polaron motion is a thermally activated process, which agrees well with our findings shown in Fig. 3. The concentration of mobile electrons is small and small-polaron conduction in Li_4C_{60} contributes significantly to the conductivity only at high frequencies, where the ionic contribution is negligible. At microwave frequencies, the

electronic (polaronic) conduction determines the conductivity. The presence of polarons can also be inferred from HREELS measurements indicating coupling of electrons to low-energy (alkali metal or intermolecular) phonons [Ref. 39].

C. Narrowing of the ESR spectrum by Li diffusion

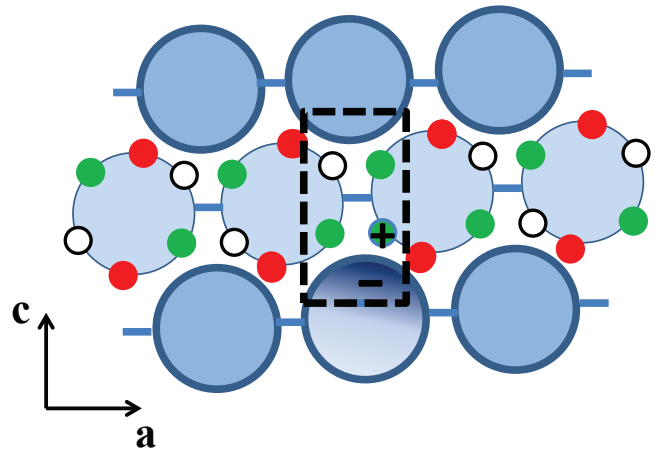


FIG. 4: Schematics of the suggested ESR active defect. Large blue circles are polymeric fulleride ions. Dark and light molecules are in the front and back, respectively. Green (red) circles are Li^+ ions in octahedral (tetragonal) sites. In stoichiometric Li_4C_{60} , octahedral voids are occupied by 2 Li^+ ions and have 2 unoccupied sites. The unpaired electron is bound to the void occupied by 3 Li^+ ions marked by a dashed line contour.

The ESR spectrum arises from defects of the polymeric matrix or from unpaired electrons in the polymeric structure bound to charges arising from a slight off-stoichiometry of the Li concentration. The ESR active defect concentration is one $S = 1/2$ spin per hundred C_{60} molecules²². As explained below, at low temperatures the large majority of the ESR active sites have the same environment and we suggest that the ESR arises mostly from off-stoichiometry. Fig. 4 is a schematic view of a charged ESR active site bound to a surplus Li^+ ion in an octahedral void. The resonance frequency of the ESR, characterized by the g -factor, is sensitive to small variations in the electronic configuration surrounding defects. The anisotropic g -shift depends on the spin-orbit interaction and the crystal field in an environment with lower than cubic symmetry and is very small in materials composed of light atoms⁴⁰. The previous ESR study²² at 35 GHz observed the deviation from cubic symmetry as a splitting of the ESR signal. The present higher resolution 222 GHz ESR work follows the evolution of the environment of ESR active defects in detail. We find that the majority of defects evolve from an axial symmetry configuration at low temperatures to an effectively isotropic configuration at ambient temperatures.

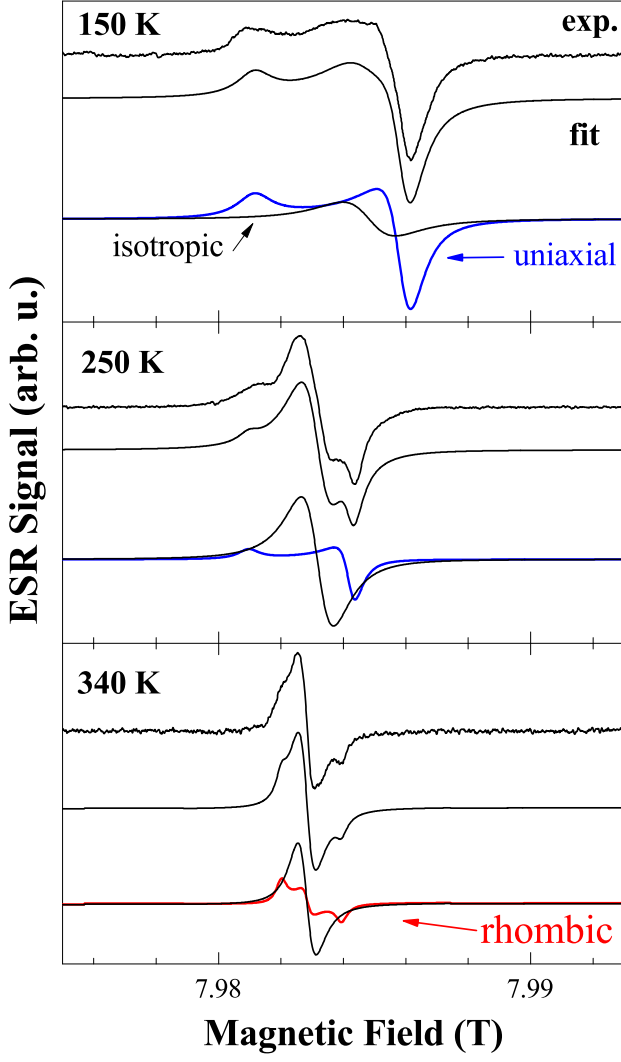


FIG. 5: Temperature evolution of the 222 GHz ESR spectrum of Li_4C_{60} . The measured experimental (exp.) and the fitted (fit) spectra are shown for each temperature. Below 290 K, the spectra consist of an isotropic (black) and a uniaxially anisotropic g -factor distribution (blue) component. Above 290 K, the anisotropic component is better described by a rhombic g -factor anisotropy (red).

Fig. 5 displays the temperature evolution of the ESR spectrum of as-prepared Li_4C_{60} . The spectrum is the superposition of ‘anisotropic’ and ‘isotropic’ components. The anisotropic component is a powder spectrum broadened by the g -factor anisotropy in the magnetic field. The line shape is characteristic of a uniaxial g -factor anisotropy (blue curve in Fig. 5)^{41,42}. The width of the anisotropic component decreases with temperature. Above 280 K only a small intensity anisotropic line with a different line shape remains that possibly reflects a lower, rhombic, symmetry. The decrease of the line width of the anisotropic component is characteristic of a fluctuating environment in which the average g -factor anisotropy is

reduced but remains finite. The isotropic component is a single line with a Lorentzian line-shape (solid line in Fig. 5), characteristic of sites with a cubic static environment or with a rapidly varying environment that averages the g -factor anisotropy to zero.

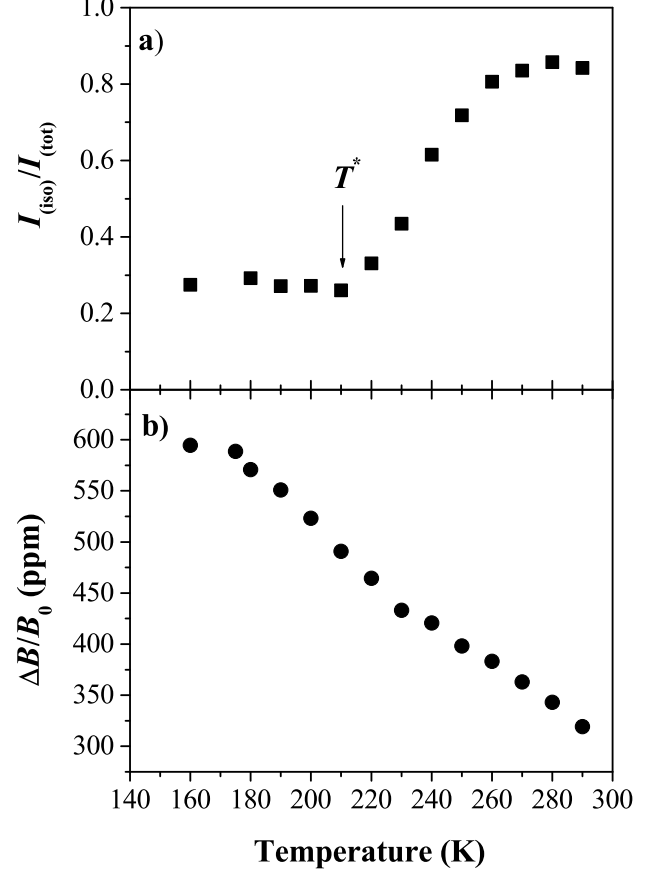


FIG. 6: a) Temperature dependence of ESR intensity of the isotropic component divided by the total one, $I_{\text{iso}}/I_{\text{tot}}$. T^* indicates the onset of Li^+ ion motion.²² b) Temperature dependence of the g -factor anisotropy, $\Delta B/B_0$, of the ESR line measured at the same frequency (222 GHz).

Fig. 6 displays the detailed variation of the relative intensity and the line width for the anisotropic component. The intensity of the isotropic component relative to the total intensity of the spectrum, $I_{\text{iso}}/I_{\text{tot}}$ is constant at low temperatures and increases in a step-like fashion between 210 and 240 K (Fig. 6a). The spectrum is dominated by the anisotropic component between 160 and 210 K and by the isotropic component above 260 K. The g -factor anisotropy of the anisotropic component decreases gradually with increasing temperature from 6.4 mT at 160 K to 2.6 mT at 290 K (Fig. 6b). The defect concentration changes less than a factor of 2 below 280 K since the spin susceptibility, measured by the ESR spectrum intensity, I_{tot} , depends little on temperature²² between 150 K and 280 K. The long elec-

tronic spin-lattice relaxation time prevents reliable intensity measurements at lower temperatures. The spin susceptibility increases rapidly above 300 K, indicating the formation of new ESR active defects.

We interpret the unusual temperature dependence of the ESR spectrum as a consequence of the fluctuation of the g -factor tensor of unpaired localized electrons arising from Li^+ motion. At low temperatures, Li ions in tetrahedral sites are static. Li ions in octahedral voids are hopping between a few possible sites and remain within voids for long times. We assume that the anisotropic component arises from unpaired electrons bound to octahedral voids with a third Li ion in addition to the two Li ions of the majority sites. (Electron holes bound to Li vacancies is another possibility). The charge of the Li ion nearest to the unpaired electron is the most important factor for the deviation from cubic symmetry of the crystal field at the unbound electron. The orientations and principal values of the g -factor tensor of a given ESR active site fluctuates between a few well defined values due to hopping of Li ions within the voids but within the ESR time scale the anisotropy is not averaged to zero. The relevant ESR time scale $\tau_{\text{ESR}} = 5 \times 10^{-9}$ s is given by the low temperature width of the anisotropic line. Non-identified sites, representing 20 percent of the localized unpaired electron defects, give a narrow, isotropic line at low temperatures.

At higher temperatures, the density of unpaired electronic states increases gradually with the increasing disorder and this decreases the effective g -factor anisotropy. At temperatures above 210 K, the fluctuations of the g -factor due to diffusion of Li ions between different voids in the polymeric structure becomes important and the line shape changes in a qualitative way. Electrons bound to (or in the vicinity of) the diffusing surplus ions experience a rapidly changing environment between many more states than experienced at lower temperatures. Diffusion involves all Li ions between voids according to Ref. 12. Each C_{60} molecule of the polymer is surrounded by 8 equidistant tetrahedral and 6 octahedral voids. Diffusion in and out the large number of sites averages the g -factor anisotropy and contributes to a narrow, on-the-average isotropic line intensity. The concentration of unpaired electrons at isotropic sites increases rapidly between 210 and 260 K but the total defect concentration does not change. Above 260 K Li ion hopping between octahedral voids determines the ESR lineshape. At 340 K only a very small intensity anisotropic line is observed around the isotropic line.

The motion of Li ions was observed in a broad temperature range by the narrowing of the ^7Li NMR spectrum²². The temperature dependence of the NMR and the ESR spectra are qualitatively similar. The NMR spectrum at low temperatures has an "anisotropic" broad component due to the distribution of electric field gradients (EFG) at octahedral Li sites. Motion of the Li ions reduces the time-averaged EFG measured by the NMR line width of the broad component. Like for the anisotropic

ESR, there are two temperature ranges. The NMR line narrows moderately with temperature up to 190 K. At higher temperatures the EFG decreases rapidly in a step-like fashion and the narrow line at high temperature is characteristic of an isotropic environment on the NMR time scale.

Microwave conductivity, ^7Li NMR, and ESR are sensitive to both intra- and inter-void hopping but at different time scales. The DC ionic conductivity senses only ion diffusion between voids. The onset of the increasing isotropic ESR signal intensity (shown with an arrow in Fig. 6) is thus associated with the onset of Li^+ ion hopping between voids around 210 K. This temperature is slightly higher than the onset temperature of the rapid narrowing of the anisotropic ^7Li NMR line. The DC ionic conductivity is more sensitive to the onset of hopping between voids and is observed from much lower temperatures. As discussed earlier, the microwave electronic conductivity is also influenced by the ionic motion.

Narrowing of the ESR spectra allows to estimate the correlation time for Li diffusion between voids as it is of the order of the correlation time, τ_m of the g -factor fluctuation⁴¹.

$$\Delta\omega_{\text{iso}}(T) = \Delta\omega^2(0) \cdot \tau_m, \quad (1)$$

where $\Delta\omega(0)$ is the width of the static low temperature anisotropic spectrum (in angular frequency units) and $\omega_{\text{iso}}(T)$ is the width of the high temperature isotropic line. Inserting $\Delta\omega(0)/\gamma = 6.4$ mT ($\gamma/2\pi = 28.0$ GHz/T is the electron gyromagnetic ratio) and $\Delta\omega_{\text{iso}}(300 \text{ K}) = 0.7$ mT, we find $\tau_m = 10^{-10}$ s.

D. Depolymerization and metallic conductivity in the monomeric phase

X-ray diffraction at high temperatures shows a depolymerization of the low temperature monoclinic polymeric phase of Li_4C_{60} into a cubic monomeric phase²⁰. The depolymerization is hysteretic; in the XRD study a mixture of monoclinic and cubic phases appears between 470 and 600 K. ESR, NMR, and Raman spectroscopy data suggests that the cubic monomer phase is metallic^{20,22}. We confirm in this work the metallic character of the high temperature phase by a direct measurement of the electronic conductivity. The structural phase transition between the electronic insulating low temperature polymeric phase and the high temperature metallic monomeric Li_4C_{60} phases is followed in the 10 GHz microwave conductivity. Fig. 7 displays two examples of the several temperature cycles performed. The heating and cooling cycle between 300 and 710 K is between the polymeric phase, well below the depolymerization temperature, to above 670 K where the material is homogeneously monomeric. In the other cycle displayed, a large part of the material remains polymeric up to 600 K.

The 10 GHz conductivity has a local maximum at 300 K and a minimum at about 400 K in all heat-

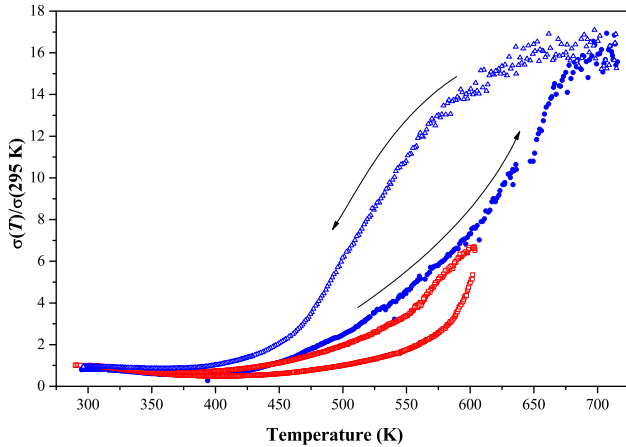


FIG. 7: Depolymerization - polymerization cycles of Li_4C_{60} measured by the 10 GHz microwave conductivity (normalized at 295 K). Full cycle: heating (blue dots) and cooling (blue triangles) rates ≈ 0.1 K/s. Partial cycle (red squares): cooling and heating rates ≈ 0.07 K/s.

ing curves with various heating rates and history. The anomaly differs little between the heating and cooling parts of the 300 and 600 K cycle where the transition to the monomer phase is only partial. Thus the maximum in the conductivity at 300 K is a feature of the polymeric phase. We suggest that the anomalous decrease in the 10 GHz electronic conductivity between 300 K and 400 K is due to the reversible breaking of some of the polymeric bonds.

Above 400 K, the conductivity increases rapidly in the heating cycle as metallic domains of the monomeric phase are formed. The hysteresis of the 10 GHz conductivity places the polymerization temperature at about 550 K in agreement with the X-ray diffraction data²⁰. For the cycle shown in Fig. 7, hysteresis is very small above 670 K. The conductivity is approximately temperature independent above this temperature and an under-cooling effect is observed well below 670 K. The monomer phase is metallic with more than an order of magnitude higher

conductivity than in the polymeric phase at ambient temperature. As expected for a metal, the spin susceptibility of the monomer phase measured by ESR is high and approximately temperature independent²². (This measurement was, however in cooling from 620 K of an incompletely polymerized sample).

IV. CONCLUSIONS

We studied the Li_4C_{60} fulleride using microwave conductivity and high field electron spin resonance spectroscopy in a wide temperature range. Low temperature microwave conductivity changes near the temperature where ionic conduction starts, which indicates a connection between the electronic and ionic conduction. HF-ESR measurements demonstrate that the Li^+ ion dynamics deeply influences the electronic configuration of the paramagnetic centers in the polymer superionic phase. For $T < 200$ K, the ions are static and localize the electrons which give rise to an ESR line with g -factor anisotropy. When Li^+ ions motion is activated, localized electrons start to diffuse with different velocities. The hopping of localized electrons gives the most important contribution to the conductivity of the polymer phase in the microwave frequency range where the ionic conductivity is negligible. Near 300 K, the conductivity has a maximum due to the onset of defect formation in the polymeric phase. The complex dynamics of the electrons in the polymer phase also results in an unusual temperature dependence of the g -factor anisotropy. Microwave conductivity measurements confirm the metallic nature of the high temperature monomeric phase Li_4C_{60} compound.

V. ACKNOWLEDGMENTS

Work supported by the ERC Starting Grant No. ERC-259374-Sylo and OTKA 105691.

* Corresponding author: f.simon@eik.bme.hu

† Present address: Semilab Semiconductor Physics Laboratory Co. Ltd., Prielle Kornélia str. 2. H-1117 Budapest, Hungary

¹ O. Chauvet, G. Oszlányi, L. Forró, P. W. Stephens, M. Tegze, G. Faigel, and A. Jánossy, Phys. Rev. Lett. **72**, 2721 (1994).

² M. Rao, P. Zhou, K. A. Wang, G. T. Hager, J. M. Holden, Y. Wang, W. T. Lee, X. X. Bi, and P. C. Eklund, Science **259**, 955 (1993).

³ M. Nunez-Regueiro, L. Marques, J.-L. Hodeau, O. Béthoux, and M. Perroux, Phys. Rev. Lett. **74**, 278 (1995).

⁴ S. Pekker, L. Forró, L. Mihály, and A. Jánossy, Solid State

Commun. **90**, 349 (1994).

⁵ G. Oszlányi, G. Baumgartner, G. Faigel, and L. Forró, Phys. Rev. Lett. **78**, 4438 (1997).

⁶ G. M. Bendeke, P. W. Stephens, K. Prassides, K. Vavakis, K. Kordatos, and K. Tanigaki, Phys. Rev. Lett. **80**, 736 (1998).

⁷ S. Margadonna, C. M. Brown, A. Lappas, K. Prassides, K. Tanigaki, K. D. Knudsen, T. L. Bihan, and M. Mézouar, J. Solid State Chem. **145**, 471 (1999).

⁸ J. O. Besenhard and G. Eichinger, J. Electroanal. Chem. **68**, 1 (1976).

⁹ S. Margadonna, D. Pontiroli, M. Belli, T. Shiroka, M. Riccò, and M. Brunelli, J. Am. Chem. Soc. **126**, 15032 (2004).

- ¹⁰ M. Riccò, T. Shiroka, M. Belli, D. Pontiroli, M. Pagliari, G. Ruani, D. Palles, S. Margadonna, and M. Tomaselli, *Phys. Rev. B* **72**, 155437 (2005).
- ¹¹ S. Rols, D. Pontiroli, C. Cavallari, M. Gaboardi, M. Aramini, D. Richard, M. R. Johnson, J. M. Zanotti, E. Suard, M. Maccarini, et al., *Phys. Rev. B* **92**, 014305 (2015).
- ¹² M. Riccò, M. Belli, M. Mazzani, D. Pontiroli, D. Quintavalle, A. Jánosy, and G. Csányi, *Phys. Rev. Lett.* **102**, 145901 (2009).
- ¹³ D. Pontiroli, M. Aramini, M. Gaboardi, M. Mazzani, A. Gorrieri, M. Riccò, I. Margiolaki, and D. Sheptyakov, *Carbon* **51**, 143 (2013).
- ¹⁴ G. Klupp, P. Matus, D. Quintavalle, L. F. Kiss, É. Kovács, N. M. Nemes, K. Kamarás, S. Pekker, and A. Jánosy, *Phys. Rev. B* **74**, 195402 (2006).
- ¹⁵ B. Sundqvist, M. Yao, and T. Wågberg, *High Pressure Research* **28**, 597 (2008).
- ¹⁶ M. Yao, T. Wågberg, and B. Sundqvist, *Phys. Rev. B* **81**, 155441 (2010).
- ¹⁷ B. Sundqvist, T. Wågberg, and M. Yao, *Diamond & Related Materials* **20**, 600 (2011).
- ¹⁸ B. Sundqvist, O. Andersson, C. Gong, B. Liu, B. Tonpheng, J. Yu, and M. Yao, *New Journal of Physics* **17**, 023010 (2015).
- ¹⁹ A. Inaba, Y. Miyazaki, P. P. Michalowski, E. Gracia-Espino, B. Sundqvist, and T. Wågberg, *The Journal of Chemical Physics* **142**, 164706 (2015).
- ²⁰ M. Riccò, M. Belli, D. Pontiroli, M. Mazzani, T. Shiroka, D. Arçon, A. Zorko, S. Margadonna, and G. Ruani, *Phys. Rev. B* **75**, 081401 (2007).
- ²¹ O. Gunnarsson, *Rev. Mod. Phys.* **69**, 575 (1997).
- ²² D. Arçon, A. Zorko, M. Mazzani, M. Belli, M. Riccò, and S. Margadonna, *New Journal Physics* **10**, 033021 (2008).
- ²³ F. Bommeli, L. Degiorgi, P. Wachter, Ö. Legeza, A. Jánosy, G. Oszlányi, O. Chauvet, and L. Forró, *Phys. Rev. B* **51**, 14794 (1995).
- ²⁴ B. Nebendahl, D.-N. Peligrad, M. Požek, A. Dulčić, and M. Mehring, *Rev. Sci. Instrum.* **72**, 1876 (2001).
- ²⁵ O. Klein, S. Donovan, M. Dressel, and G. Gruner, *International Journal of Infrared and Millimeter Waves* **14**, 2423 (1993).
- ²⁶ L. I. Buravov and I. F. Shchegolev, *Instrum. Exp. Tech.* **14**, 528 (1971).
- ²⁷ K. L. Nagy, D. Quintavalle, T. Fehér, and A. Jánosy, *Applied Magnetic Resonance* **40**, 47 (2011).
- ²⁸ G. Oszlányi, G. Baumgartner, G. Faigel, and L. Forró, *Phys. Rev. Lett.* **78**, 4438 (1997).
- ²⁹ V. C. Long, J. L. Musfeldt, K. Kamarás, G. B. Adams, J. B. Page, Y. Iwasa, and W. E. Mayo, *Phys. Rev. B* **61**, 13191 (2000).
- ³⁰ G. Klupp, K. Kamarás, N. M. Nemes, C. M. Brown, and J. Leao, *Phys. Rev. B* **73**, 085415 (2006).
- ³¹ D. Quintavalle, F. Borondics, G. Klupp, A. Baserga, F. Simon, A. Jánosy, K. Kamarás, and S. Pekker, *Phys. Rev. B* **77**, 155431 (2008).
- ³² R. H. Zadik, Y. Takabayashi, G. Klupp, R. H. Colman, A. Y. Ganin, A. Potocnik, P. Jeglic, D. Arçon, P. Matus, K. Kamarás, et al., *Sci. Advances* **1**, e1500059 (2015).
- ³³ K. Kamarás and G. Klupp, *Dalton Trans.* **43**, 7366 (2014).
- ³⁴ A. S. Cattaneo, V. Dall'Asta, D. Pontiroli, M. Riccò, G. Magnani, C. Milanese, C. Tealdi, E. Quartarone, and P. Mustarelli, *J. Mat. Chem. A* **submitted** (2016).
- ³⁵ C. Kittel, *Introduction to Solid State Physics* (Wiley, New York, 1986), VIth ed.
- ³⁶ J. Sólyom, *Fundamentals of the Physics of Solids: Volume II - Electronic Properties* (Springer, Berlin, 2009).
- ³⁷ T. Holstein, *Ann. Phys.* **8**, 325 (1959).
- ³⁸ M. Jaime, H. T. Hardner, M. B. Salamon, M. Rubinstein, P. Dorsey, and D. Emin, *Phys. Rev. Lett.* **78**, 951 (1997).
- ³⁹ R. Macovez, R. Savage, L. Venema, J. Schiessling, K. Kamarás, and P. Rudolf, *J. Phys. Chem. C* **112**, 2988 (2008).
- ⁴⁰ P. Fazekas, *Lecture Notes on Electron Correlation and Magnetism*, Series in Modern Condensed Matter Physics (World Scientific, 1999).
- ⁴¹ C. P. Slichter, *Principles of Magnetic Resonance* (Springer-Verlag, New York, 1989), 3rd ed.
- ⁴² N. M. Atherton, *Electron Spin Resonance; Theory and Applications* (E. Horwood; Halsted Press Chichester New York, 1973).